

Supporting Information for:

BaTiO₃ Thin Films from Atomic Layer Deposition: A Superlattice Approach

Matthias Falmbigl¹, Irina S. Golovina^{1,2}, Aleksandr V. Plokhikh¹, Dominic Imbrenda³, Adrian Podpirka¹, Christopher J. Hawley¹, Geoffrey Xiao¹, Alejandro Gutierrez-Perez¹, Igor A. Karateev⁴, Alexander L. Vasiliev⁴, Thomas C. Parker⁵, and Jonathan E. Spanier^{1,3,6}

¹*Department of Materials Science & Engineering, Drexel University, Philadelphia, Pennsylvania 19104, USA*

²*Institute of Semiconductor Physics of NAS of Ukraine, Pr. Nauki 41, Kiev 03028, Ukraine*

³*Department of Electrical & Computer Engineering, Drexel University, Philadelphia, Pennsylvania 19104, USA*

⁴*National Research Center “Kurchatov Institute”, Kurchatov Square 1, Moscow 123182, Russia*

⁵*US Army Research Laboratory, Aberdeen Proving Ground, Maryland 21005, USA*

⁶*Department of Physics, Drexel University, Philadelphia, Pennsylvania 19104, USA*

ALD-Growth

In a first step the growth characteristics of TiO₂ from Ti-isopropoxide (TTIP) and H₂O were established at T_{RC}= 290°C (temperature in the reaction chamber), which is within the reported ALD window for this precursor.¹ Two sets of samples were deposited on Si-substrates. In the first set the pulse time for TTIP was varied, while the purge time for TTIP and the pulse and purge time for H₂O were kept constant at 1 s, 1 s, and 3 s, respectively. For the second set of samples the pulse time of water was varied, while the pulse and purge time for TTIP and the purge time for H₂O were kept constant at 0.3 s, 1 s, and 3 s, respectively (see Fig. S1). A saturated growth rate (GPC, growth per cycle) of 0.35 Å with a slight increase for longer water doses was found, which is consistent with previous literature reports for this well investigated binary system (see Fig. S1).¹⁻⁴ An *in situ* crystallization experiment revealed the formation of TiO₂ in the anatase structure during the deposition process and no changes in the X-ray diffraction patterns upon annealing up to 700°C, again in agreement with literature reports for ALD-grown TiO₂ in a similar deposition temperature range.^{5,6}

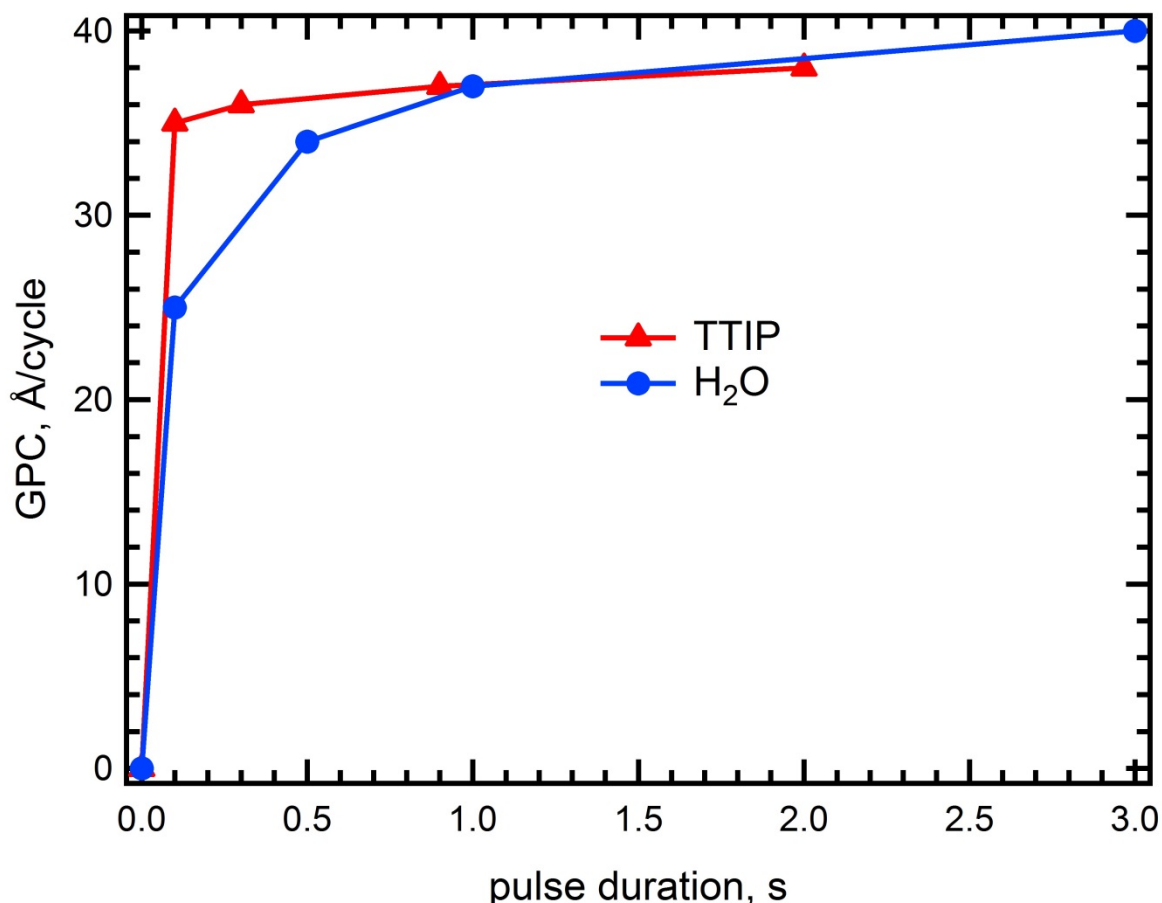


Fig. S1. Growth per cycle for TiO₂ from Ti-isopropoxide (TTIP) and H₂O.

TiO₂ growth using TTIP and H₂O at T_{RC}= 290°C results in an extremely uniform film thickness (>98 % over an area of 200 mm diameter). In order to maintain this high uniformity for the ternary films the influence of the number of consecutive Ba(Cp)₂ pulses (k) on the deposition process was investigated. The results are summarized in Fig. S2a and S2b. The growth per Ba-pulse for the Ba-O subcycle is 0.7 Å for $k=1$. The GPC decreases constantly to 0.31 Å for 6 Ba-pulses (Fig. S2b). The increase of the film thickness as well as the Ba/Ti-ratio with increasing k clearly demonstrate that the Ba-O layer retains a significant amount of hydrate on the growing surface, Ba(OH)₂· n H₂O,⁷ after the H₂O pulse, although the pulse and purge times of 0.1 s and 10 s are already adjusted to ensure the removal of all volatile species before the following pulse. This increase could partially also arise from the effect of reduced steric hindrance through chemisorbed species as theoretically predicted and demonstrated for different binary ALD processes.⁸ The hydrate formation leads to the loss of a truly self-terminating growth on the film surface. Although, even at $k=6$ there is still hydrate present as evident from a further thickness increase as compared to $k=4$ (Fig. S2a), this pulsing sequence proves to effectively mitigate uncontrolled reactions and the incorporation of H₂O into the film. The uniformity probed over a length of 100 mm exhibits a maximum for $k=4$ (Fig. 1b). The initial improvement in uniformity arises from an increasingly conformal coverage and adsorption of the deposition area by

Absolut-Ba due to gas phase saturation in the reaction chamber. The slight decrease from $k=4$ to 6 can be attributed to localized precursor oversaturation in the deposition chamber.

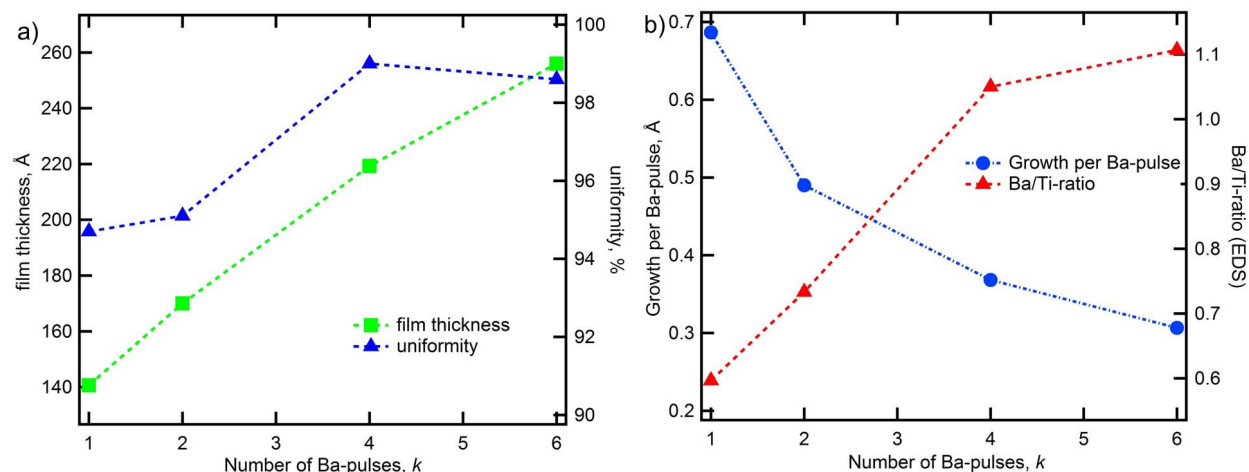


Fig. S2. a) Film thickness from XRR scans and uniformity on a 100 mm wafer as a function of the number of consecutive Ba(Cp)₂ pulses (k), b) Growth per Ba-pulse and Ba/Ti-ratio as a function of the number of consecutive Ba(Cp)₂ pulses (k).

The uniformity of the atomic layer deposition process was tested for the area of a 200 mm wafer distributing 9 Si coupons as displayed in the schematic in Fig. S2a. The deposition sequence, $(\text{TTIP-H}_2\text{O}) \times 40 + [(4 \times \text{iPr}_3\text{Cp-H}_2\text{O}) \times 25 + (\text{TTIP-H}_2\text{O}) \times 50] \times 20$, resulted in a 1100 Å thick film with Ba/Ti-ratio of 1. The thickness was extracted from XRR scans and revealed a uniformity of 99.8 % for a diameter of 100 mm and a uniformity of 98.8 % in the area of a 200 mm wafer. The uniformity was evaluated for 100 and 200 mm diameter wafers by distributing 9 Si coupons as displayed in Fig. S3a over the sample holder. The thickness of each coupon was evaluated from XRR-scans and three representative scans are depicted in Fig. S3b.

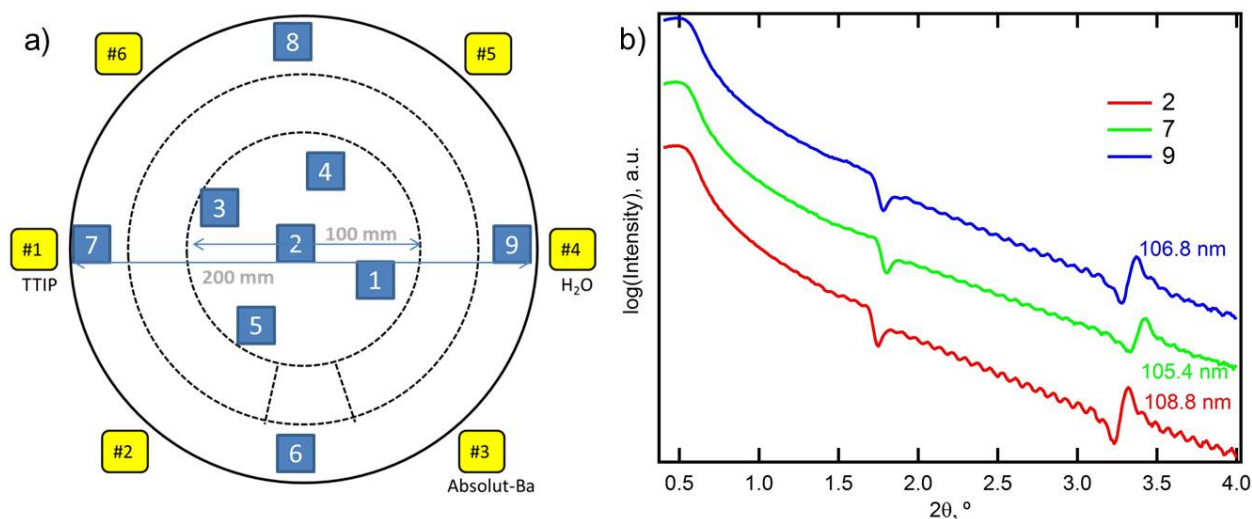


Fig. S3. a) Schematic of the positions of 9 Si coupons distributed over the area of a 200 mm wafer on the sample holder of the ALD chamber, and b) Representative X-ray reflectivity data for three coupons. The numbers correspond to the positions indicated in Fig. S3a.

X-ray Reflectivity

In-situ XRR as a function of temperature was utilized to monitor the thickness change of the 1100 Å thick film. A marginal decrease up to 500°C is followed by a 10 % decrease further up to 550°C (Fig. S4a). This shrinking coincides with the formation of BaTiO₃ from the semi-amorphous superlattice. Fitting of the XRR-data at 200°C and 700°C confirms that the deposition at T_{RC}= 290°C results in a superlattice with a reproducible thickness of the individual Ba-O and Ti-O subunits for 20 repeats. Upon annealing this superlattice forms a homogeneous BaTiO₃ film (see Fig. S4b).

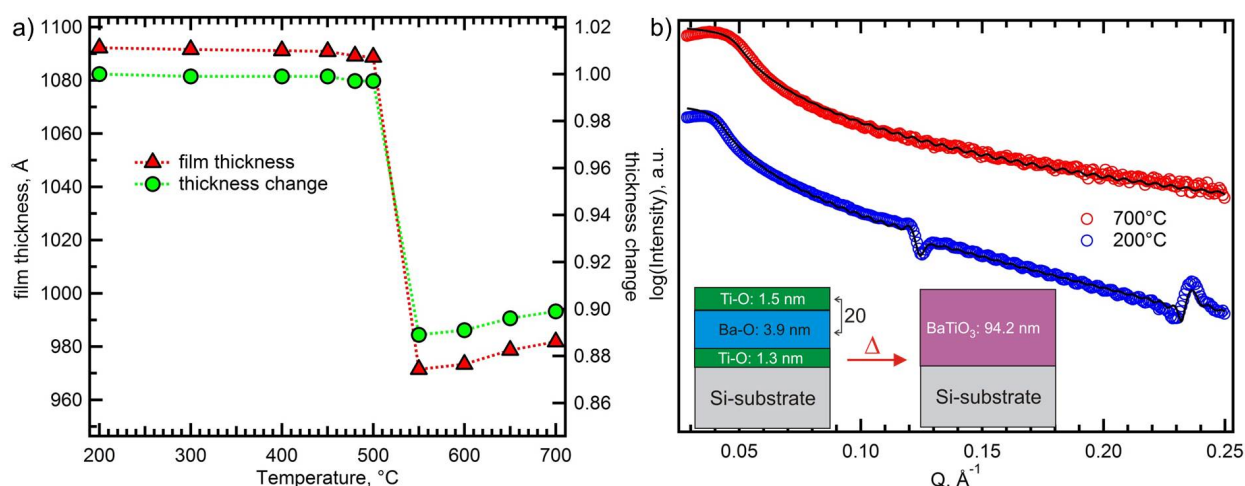


Fig. S4. a) Film thickness and relative thickness change as a function of temperature extracted from XRR-data, and b) XRR scans at 200°C and 700°C with corresponding fits (black solid lines) that represent the two models in the schematic.

Rutherford Backscattering Spectroscopy

The RBS data collected on the 1100 Å thick film deposited on a Si-substrate before and after the in-situ X-ray diffraction experiment are displayed in Fig. S5. For the simulation of the data of the as deposited film an average density of 4.3 Mgm⁻³ calculated from the layer thickness and corresponding densities of TiO₂ ($\rho = 3.88 \text{ Mgm}^{-3}$) and $\alpha\text{-Ba(OH)}_2$ ($\rho = 4.4 \text{ Mgm}^{-3}$)⁹ was used. This resulted in a total film thickness of 1118 Å, which is in excellent agreement with 1088 Å from XRR.

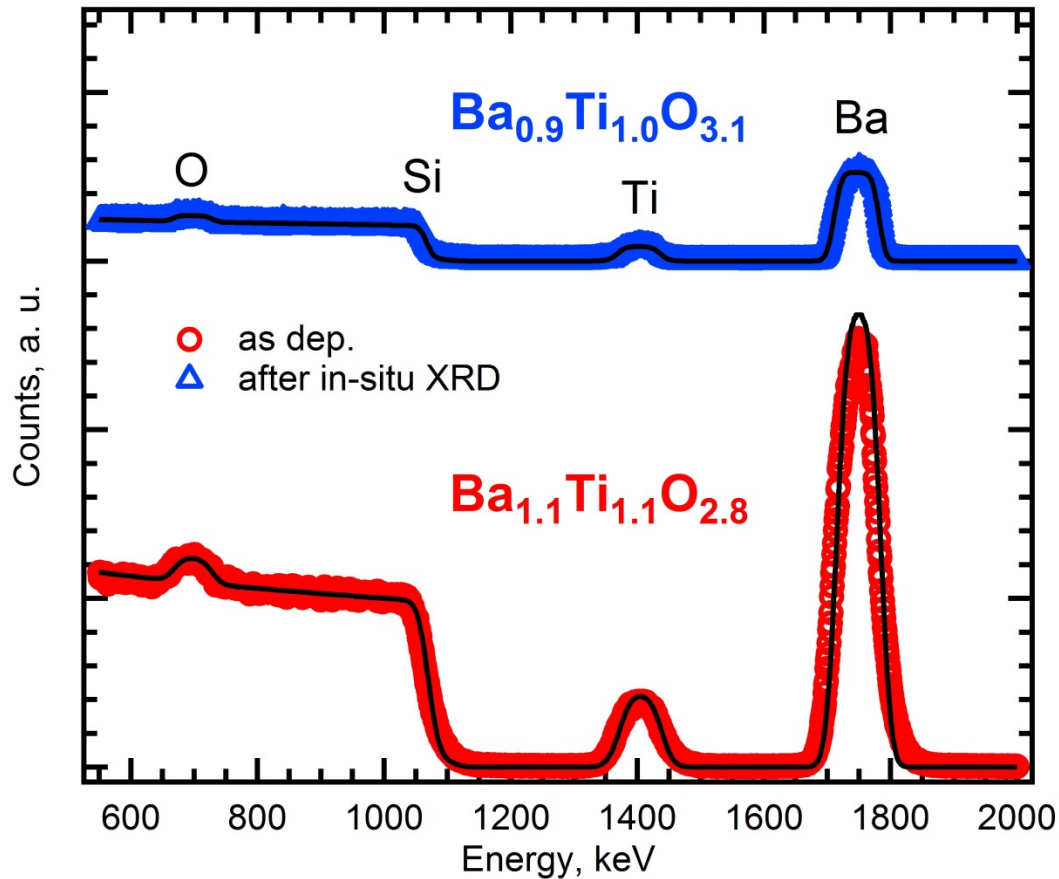


Fig. S5. Rutherford backscattering spectroscopy data for the 1100 Å thick film on Si after the deposition (red) and after the *in-situ* XRD experiment (blue). The black lines represent the simulated data.

Transmission Electron Microscopy

Fig. S6 depicts a bright field (BF) TEM image and selected area electron diffraction (SAED) from the *in-situ* experiment at 450°C. The superlattice structure is still visible throughout the film implying that the cations are still segregated into individual layers. Also the total film thickness is within error still similar to the as-grown film, which is in excellent agreement with the results from XRR (see Fig. S4a). These observations are corroborated by SAED (Fig. S6b), where besides the substrate reflections only Debye-Scherrer rings corresponding to polycrystalline α -Ba(OH)₂ are present.⁹ The SAED is still similar to the electron diffraction collected before the annealing experiment started.

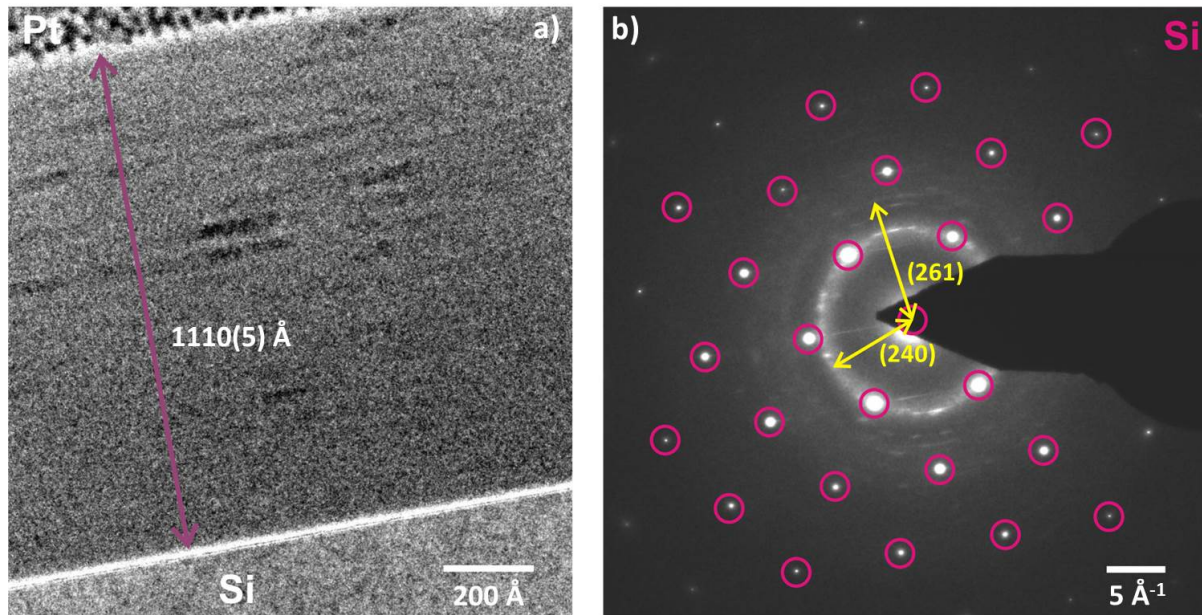


Fig. S6. a) BF-TEM image of the film at 450°C, and b) Selected area electron diffraction at 450°C with reflections from the Si-substrate and diffraction rings indexed to α -Ba(OH)₂.⁹

In Fig. S7 a HAADF-STEM image for the film annealed *ex situ* at 600°C for 2h is shown. Two areas for energy dispersive spectroscopy (EDS) were measured and a similar cation ratio within error is found. The discrepancy from the expected Ba/Ti-ratio of 1 might arise from the overlapping of the Ba_{Lα}(4.46(4) keV) and Ti K_α(4.50(7) keV) X-ray emission lines. The TEM image in Fig. S7 b) displays a cross section covering the entire film thickness after 650°C. Crystalline areas are clearly visible and the film thickness of 1030(5) Å is similar to the thickness at 500°C. Again, this is consistent with the temperature dependence of the film thickness extracted from XRR-data (see Fig. S4 a)). The SAED after 650°C displayed in Fig. S7c exhibits reflection rings that can be indexed to cubic BTO and confirm the polycrystallinity of the film. In addition, within the (110) ring of the perovskite phase there are additional reflections indicating the presence of h-BTO or a tetragonal distortion. This observation points towards a relatively high density of h- and/or t-BTO after 650°C.

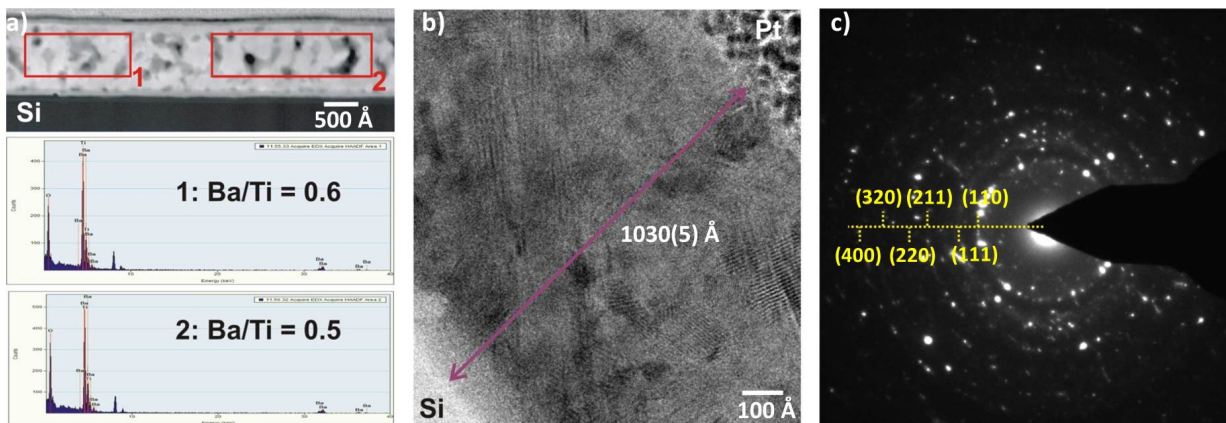


Fig. S7. a) HAADF-STEM image after annealing at 600°C with EDS spectra collected for two areas, b) HR-TEM image of the film after 650°C, and c) SAED after 650°C with diffraction rings and selected Miller indices for cubic BaTiO₃.

X-ray diffraction for MIM structures

GI-XRD scans in Fig. S8 show the formation of polycrystalline BTO films on Pt(111)/Ti/SiO₂/Si(100) substrates from the as-grown state to annealing at 500°C and 600°C in air for 1h. All peaks of the annealed samples can be indexed to cubic BTO with additional peaks from the polycrystalline Pt top electrodes. The relatively weak intensity and large full width at half maximum (FWHM) do not permit a distinction between cubic and tetragonal symmetry of BaTiO₃.

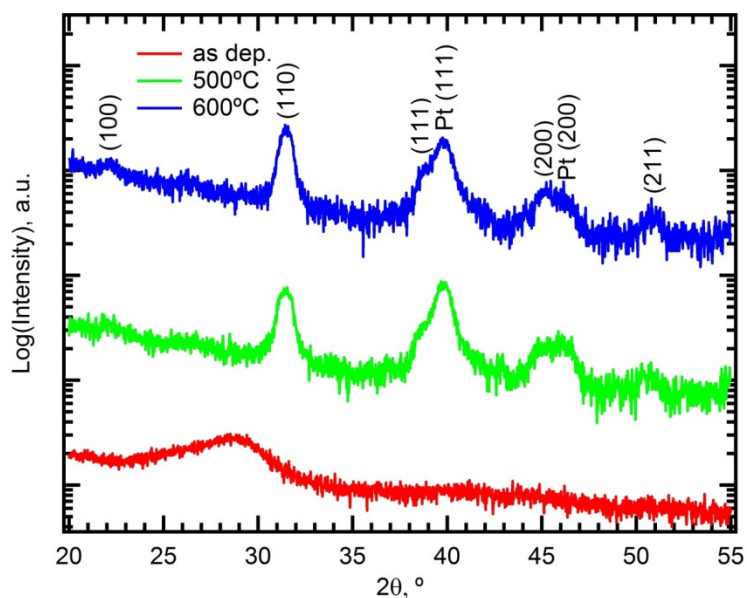


Fig. S8. GI-XRD scans of the 1100 Å thick BTO films on Pt(111)/Ti/SiO₂/Si(100) substrates. The Miller indices for cubic BTO and Pt (from the top electrodes) are provided.

References:

- (1) Ritala, M.; Leskela, M.; Niinisto, L.; Haussalo, P.; Niinist, L. *Chem. Mater.* **1993**, *5* (8), 1174.
- (2) Matero, R.; Rahtu, A.; Ritala, M.; Leskelä, M.; Sajavaara, T. *Thin Solid Films* **2000**, *368* (2000), 1.
- (3) Aarik, J.; Aidla, A.; Sammelselg, V.; Uustare, T.; Ritala, M.; Leskelä, M. *Appl. Surf. Sci.* **2000**, *161*, 385.
- (4) Rahtu, A.; Ritala, M. *Chem. Vap. Depos.* **2002**, *8* (1), 21.
- (5) Pore, V.; Rahtu, A.; Leskelä, M.; Ritala, M.; Sajavaara, T.; Keinonen, J. *Chem. Vap. Depos.* **2004**, *10* (3), 143.
- (6) Alekhin, A. P.; Gudkova, S. A.; Markeev, A. M.; Mitiaev, A. S.; Sigarev, A. A.; Toknova, V. F. *Appl. Surf. Sci.* **2010**, *257* (1), 186.
- (7) Lutz, H. D.; Eckers, W.; Christian, H.; Engelen, B. *Thermochim. Acta* **1981**, *44*, 337.
- (8) Muneshwar, T.; Cadien, K. *J. Appl. Phys.* **2016**, *119* (8).
- (9) Buck, P.; Bärnighausen, H. *Acta Crystallogr. Sect. B Struct. Crystallogr. Cryst. Chem.* **1968**, *24* (12), 1705.